J|A|C|S
ARTICLES

Published on Web 06/17/2009

Elucidating the Mechanism of Lipid Membrane-Induced IAPP Fibrillogenesis and Its Inhibition by the Red Wine Compound Resveratrol: A Synchrotron X-ray Reflectivity Study

Florian Evers,[†] Christoph Jeworrek,[‡] Sebastian Tiemeyer,[†] Katrin Weise,[‡] Daniel Sellin,[‡] Michael Paulus,[†] Bernd Struth,[§] Metin Tolan,[†] and Roland Winter*[,‡]

Faculty of Chemistry, TU Dortmund, 44221 Dortmund, Germany, Faculty of Physics/DELTA, TU Dortmund, 44221 Dortmund, Germany, and Deutsches Elektronen-Synchrotron, HASYLAB, Notkestr. 85, 22607 Hamburg, Germany

Received December 14, 2008; E-mail: roland.winter@tu-dortmund.de

Abstract: The islet amyloid polypeptide (IAPP) or amylin is a pancreatic hormone and crucially involved in the pathogenesis of type-II diabetes mellitus (T2DM). Aggregation and amyloid formation of IAPP is considered as the primary culprit for pancreatic β-cell loss in T2DM patients. In this study, first X-ray reflectivity (XRR) measurements on IAPP at lipid interfaces have been carried out, providing a molecular level characterization of the first steps of the lipid-induced fibrillation process of IAPP, which is initiated by lipid-induced nucleation, oligomerization, followed by detachment of larger IAPP aggregate structures from the lipid membrane, and terminated by the formation of mature fibrils in the bulk solution. The adsorption process of IAPP at lipid interfaces in the absence and presence of negatively charged lipid has also been studied by complementary ATR-FTIR spectroscopic measurements. The morphological properties were followed by atomic force microscopy (AFM). Moreover, we show that the polyphenolic red wine compound resveratrol is able to inhibit IAPP aggregation also in the presence of aggregation-fostering negatively charged lipid interfaces, revealing its potential as a drug candidate for T2DM.

1. Introduction

In a biological cell, proteins adopt a functional folded state which results from highly regulated processes. Upon failure of the quality control of the cell, proteins may suffer from degradation and can form assemblies of unfolded or partially folded monomers or protein fragments, such as ordered cross-β-sheet rich structures called amyloid fibrils.[1,2] Misfolding, aggregation, and fibril formation of proteins such as Aβ, α-synuclein or islet amyloid polypeptide (IAPP) have severe implications in neurodegenerative diseases like Alzheimer's and Parkinson's disease or in affecting peripheral tissues as in the case of diabetes mellitus.[1−7]

In type-II diabetes mellitus (T2DM), extracellular amyloid plaques are deposited near pancreatic beta cells. Biochemical analysis has shown that these plaques consist mainly of the 37 residue IAPP, which is co-secreted with insulin.[8] In its native state, several functions have been associated with IAPP, in particular controlling hyperglycemia by regulating the blood glucose level.[9] The mechanism of the fibrillation of IAPP that triggers its conversion from a functional soluble monomer into insoluble amyloid fibrils is still under debate. Several studies have shown that the interaction of IAPP with lipid membranes may induce fibril formation.[6,7,10,11] It has also been shown that human IAPP (hIAPP) aggregation and fibrillation in the presence of anionic lipid membranes is drastically fostered and occurs via insertion of the N-terminal region of hIAPP.[10−13] Despite recent efforts toward a biophysical characterization of the different states of aggregation,[6−14] the lack of structural information still hampers the understanding of its fibrillogenesis.

Inhibiting amyloid fibril formation is regarded as a potentially key therapeutic approach toward amyloid-related diseases.[1,2] Although the process of inhibition is not fully understood yet,

[†] Faculty of Physics, TU Dortmund University.
[‡] Faculty of Chemistry, TU Dortmund University.
[§] HASYLAB.

(1) Chiti, F.; Dobson, C. M. *Annu. Rev. Biochem.* **2006**, *75*, 333–366.
(2) Cohen, F. E.; Kelly, J. W. *Nature* **2003**, *426*, 905–909.
(3) Ege, C.; Majewski, J.; Wu, G.; Kjaer, K.; Lee, K. Y. C. *ChemPhysChem* **2005**, *6*, 226–229.
(4) Yan, L.-M.; Velkova, A.; Tatarek-Nossol, M.; Andreetto, E.; Kapurniotu, A. *Angew. Chem., Int. Ed.* **2007**, *46*, 1246–1252.
(5) Velkova, A.; Tatarek-Nossol, M.; Andreetto, E.; Kapurniotu, A. *Angew. Chem., Int. Ed.* **2008**, *47*, 7114–7118.
(6) Sparr, E.; Engel, M. F. M.; Sakharov, D. V.; Sprong, M.; Jacobs, J.; de Kruijff, B.; Höppener, J. W. M.; Killian, J. A. *FEBS Lett.* **2004**, *577*, 117–120.
(7) Engel, M. F. M.; Khemtémourian, L.; Kleijer, C. C.; Meeldijk, H. J. D.; Jacobs, J.; Verkleij, A. J.; de Kruijff, B.; Killian, J. A.; Höppener, J. W. M. *Proc. Natl. Acad. Sci. U.S.A.* **2008**, *105*, 6033–6038.
(8) Westermark, P.; Wernstedt, C.; Wilander, E.; Hayden, D. W.; O'Brien, T. D.; Johnson, K. H. *Proc. Natl. Acad. Sci. U.S.A.* **1987**, *84*, 3881–3885.
(9) Marzban, L.; Park, K.; Verchere, C. B. *Exp. Gerontol.* **2003**, *38*, 347–351.
(10) Engel, M. F. M.; Yigittop, H.; Elgersma, R. C.; Rijkers, D. T. S.; Liskamp, R. M. J.; de Kruijff, B.; Höppener, J. W. M.; Killian, J. A. *J. Mol. Biol.* **2006**, *356*, 783–789.
(11) Lopes, D. H. J.; Meister, A.; Gohlke, A.; Hauser, A.; Blume, A.; Winter, R. *Biophys. J.* **2007**, *93*, 3132–3141.
(12) Jeworrek, C.; Hollmann, O.; Steitz, R.; Winter, R.; Czeslik, C. *Biophys. J.* **2009**, *96*, 1115–1123.
(13) Williamson, J. A.; Miranker, A. D. *Protein Sci.* **2007**, *16*, 110–117.
(14) Vaiana, S. M.; Ghirlando, R.; Yau, W. M.; Eaton, W. A.; Hofrichter, J. *Biophys. J.* **2008**, *94*, L45–L47.

10.1021/ja8097417 CCC: $40.75

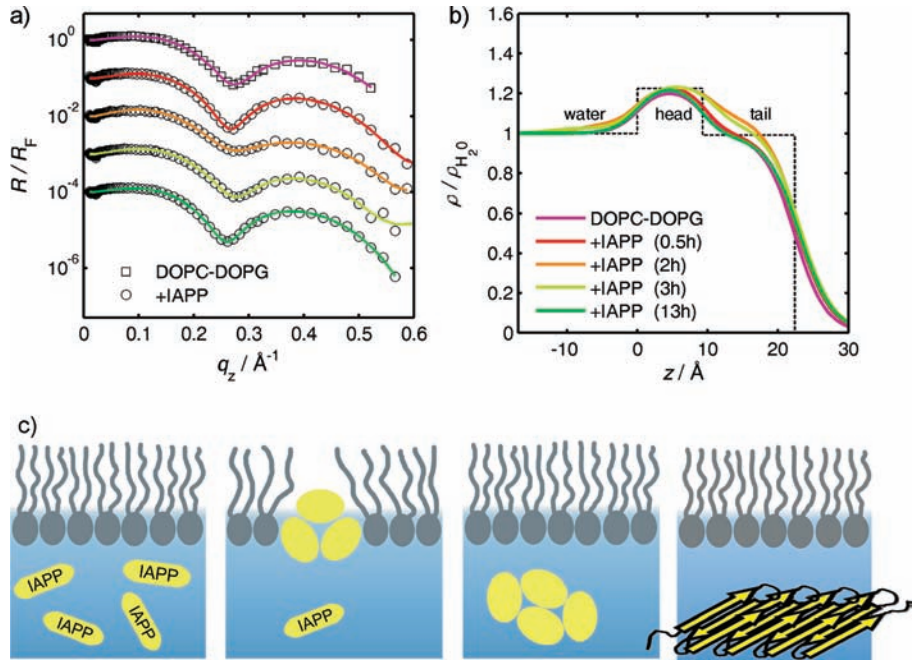

Figure 1. Association of IAPP with a negatively charged DOPC/DOPG lipid film at the air−water interface. (a) Normalized XRR data (dotted) and refinement (solid lines) at different times (vertically shifted for better visibility by 1 order of magnitude). (b) Corresponding normalized electron density profiles. (c) Schematic illustration of the time-evolution of the lipid-induced IAPP aggregation process: IAPP in bulk solvent, adsorption and oligomerization at the anionic lipid interface, detachment of larger aggregate structures and fibril formation (yellow arrows: cross β-sheet arrangement of fibrils) at IAPP concentrations >5 μM.

screening of inhibitors turned out to be beneficial.[15,16] Polyphenols are a group of compounds which have been found to act as inhibitors of Aβ, α-synuclein, and prion amyloid formation.[17] The phenolic compound resveratrol (trans-3,5,4′-trihydroxystilben), which is found to a significant amount in red wine (130−220 μM), effectively inhibits Aβ (25−35) fibril formation and reduces the secreted and intracellular Aβ level.[18] Since IAPP and Aβ have similar amino acid sequences in the presumable ordered region and exhibit similar secondary structures in the fibrillar state,[19] one may speculate on a similar inhibitory effect of resveratrol on IAPP fibril formation. This presumption has been explored in this study as well.

2. Experimental Details

2.1. Materials. Human IAPP was obtained from Calbiochem (Darmstadt, Germany). NaH_2PO_4, Na_2HPO_4, resveratrol, 2,2,2-trifluoroethanol (TFE), and 1,1,1,3,3,3-hexafluoroisopropanol (HFIP) were purchased from Sigma-Aldrich (Steinheim, Germany). 1,2-Dioleoyl-*sn*-glycero-3-phosphocholine (DOPC) and 1,2-dioleoyl-*sn*-glycero-3-[phospho-*rac*-(1-glycerol)] (DOPG) were from Avanti Polar Lipids (Alabaster, AL). D_2O and chloroform were obtained from Merck (Darmstadt, Germany). The reagents used were of the highest analytical grade available and used without further purification.

2.2. Peptide Solutions. An amount of 0.5 mg of hIAPP was initially dissolved in 1 mL of tetrafluorethanol (TFE) or hexafluoroisopropanol (HFIP) and afterward in buffer, a procedure that dissolves any preformed fibrils. A total of 500 μL of this solution was dried at the inner side of a round-bottom flask using a gentle stream of nitrogen. Then, a phosphate buffer solution (10 mM, pH 7.0) was added to obtain an IAPP sample solution for the X-ray reflectivity (XRR) and atomic force microscopy (AFM) measurements with a concentration of 1 μM. The IAPP for the ATR-FTIR measurements was dissolved in HFIP. A total of 100 μL of the stock solution was freeze-dried and the peptide was dissolved in 1 mL of D_2O buffer (10 mM PO_4^{3-}, pH 7.4, NaCl, total ionic strength: 100 mM) to obtain a final concentration of 10 μM. For the samples including resveratrol, the inhibitor was dissolved in the buffer yielding a resveratrol/IAPP molar ratio of 1.5. All IAPP solutions were used immediately after preparation for the X-ray reflectivity measurements.

2.3. X-ray Reflectivity Measurements. To reveal structural details of protein−lipid films with Angstroem resolution, resorting to X-ray scattering techniques is very beneficial. In particular, determination of the vertical electron density profile of soft matter thin films is made possible by XRR experiments.[3,20] A lipid monolayer of neutral, zwitterionic dioleoyl-phosphatidylcholine (DOPC) and the anionic dioleoyl-phosphatidylglycerine (DOPG) (in the ratio 7:3) was spread on a phosphate buffer solution in a Langmuir trough. The 7:3 ratio was chosen because it resembles the ratio of zwitterionic lipids to negatively charged lipids of the membrane of pancreatic islet cells.[21] The lipid monolayers were compressed to 30 mN/m mimicking the film pressure of physiological cell membranes. Since the incoming and reflected X-ray beams are symmetrically arranged in a reflectivity experiment, the wavevector transfer, q_z, has only a vertical component which is given by $q_z = (4\pi/\lambda)\sin\Theta$. Here, λ and Θ denote the wavelength of the radiation and the angle between the surface and the X-ray beam, respectively. Thus, the XRR technique provides detailed information on the electron density profile (EDP), $\rho(z)$, perpendicular to the membrane plane (z-direction), laterally averaged over

(15) Mishra, R.; Bulic, B.; Sellin, D.; Jha, S.; Waldmann, H.; Winter, R. *Angew. Chem., Int. Ed.* **2008**, *47*, 4679–4682.
(16) Bulic, B.; Pickhardt, M.; Khlistunova, I.; Biernat, J.; Mandelkow, E. M.; Mandelkow, E.; Waldmann, H. *Angew. Chem., Int. Ed.* **2007**, *46*, 9215–9219.
(17) Porat, Y.; Abramowitz, A.; Gazit, E. *Chem. Biol. Drug Des.* **2006**, *67*, 27–37.
(18) Marambaud, P.; Zhao, H.; Davies, P. *J. Biol. Chem.* **2005**, *280*, 37377–37382.
(19) Jayasinghe, S. A.; Langen, R. *J. Biol. Chem.* **2004**, *279*, 48420–48425.
(20) Evers, F.; Shokuie, K.; Paulus, M.; Sternemann, C.; Czeslik, C.; Tolan, M. *Langmuir* **2008**, *24*, 10216–10221.
(21) Rustenbeck, I.; Matthies, A.; Lenzen, S. *Lipids* **1994**, *29*, 685–692.

the entire lipid film (*xy*-plane).[22,23] Reflectivity measurements are predominantly sensitive to electron density differences, and consequently, investigating the interfacial structure of low-contrast organic materials, as for example present in biological systems, poses a great challenge.[20,24]

The raw data were background corrected, normalized, and scaled as a function of q_z. Reflectivity data are presented in the form R/R_F versus q_z. Thus, the strong decrease of the Fresnel reflectivity, R_F, of a sharp air-subphase interface with q_z^{-4} is compensated and features of the reflectivity curves stemming from the lipid monolayer and the associated proteins are highlighted. To extract information on the EDP from the reflectivity data, a model of the vertical structure of the studied system is proposed from which a model reflectivity is calculated by Parratt's recursive method. The most common approach to describe the EDP is to use a stack of homogeneous layers each with a distinct electron density, ρ, and layer thickness, d. The interfacial roughness, σ, between adjacent layers is accounted for as well. The simplest, physically reasonable model for lipid Langmuir films consists of two layers representing the lipid headgroup and tail, respectively. In the case of IAPP association at DOPC/DOPG lipid films, the data interpretation in terms of a two-layer model is insufficient. A third layer is introduced accounting for the peptide protruding into the subphase. By resorting to the simplest box model that explains the XRR data well, it is reassured that the profiles are not overparameterized. The refinement of the data was performed using the program LSFIT,[23] a least-squares fitting routine applying the Levenberg−Marquardt algorithm. The EDP is described in terms of the effective density model which assures for continuous profiles even if the roughness is not very small compared to the layer thickness.[23] The accuracy of the parameters retrieved from the refinement of the data is assessed by varying the parameters manually and observing the corresponding effect on the calculated reflectivity curve. The typical accuracy of the fitting parameters is estimated to ± 0.03 e/Å^3 for ρ, ± 0.1 Å for d, and ± 0.3 Å for σ. All fitting parameter are depicted in Tables 1−III (Supporting Information).

The X-ray reflectivity measurements were performed at the liquid surface diffractometer of beamline BW1 at HASYLAB (Hamburg, Germany). The beamline was equipped with a temperature-controlled Langmuir trough in a sealed container. A Wilhelmy film balance for measuring the surface pressure, π, and a Teflon barrier for changing the surface area, A, were installed in the trough. During the experiments, the container was flushed with helium in order to suppress air-scattering and to prevent oxidative beam damage during X-ray scans. All experiments were carried out at 22 °C. The samples were illuminated with an X-ray beam with a wavelength, λ, of 1.3 Å, corresponding to a photon energy, E, of 9.5 keV. One reflectivity scan took 35 min, reached a maximum wavevector transfer, q_z, of 0.7 Å^{-1}, and covered a dynamic range of 10 orders of magnitude. The starting point of an experiment ($t = 0$ h) was defined as the time point when the sample system was prepared on the Langmuir trough.

2.4. Atomic Force Microscopy. For the AFM measurements, the entire solution in the Langmuir trough was transferred to a glass separating funnel at particular time points of the experiment and extracted four times with each 5 mL of chloroform to remove the lipids from the aqueous phase. To reveal structural details of hIAPP in the DOPC/DOPG monolayer after 3 h, the lipid film was carefully withdrawn from the aqueous subphase in the Langmuir trough with a glass syringe and lipids were removed by chloroform extraction as described above to isolate the existing hIAPP species. The buffer solutions were collected and 120 μL of the sample was deposited on freshly cleaved muscovite mica, allowed to incubate for a few minutes and dried immediately with a nitrogen stream. Afterward, the sample was rinsed carefully with about 6 mL of deionized water and dried again with a nitrogen stream; all solvent was subsequently removed by drying under vacuum overnight.

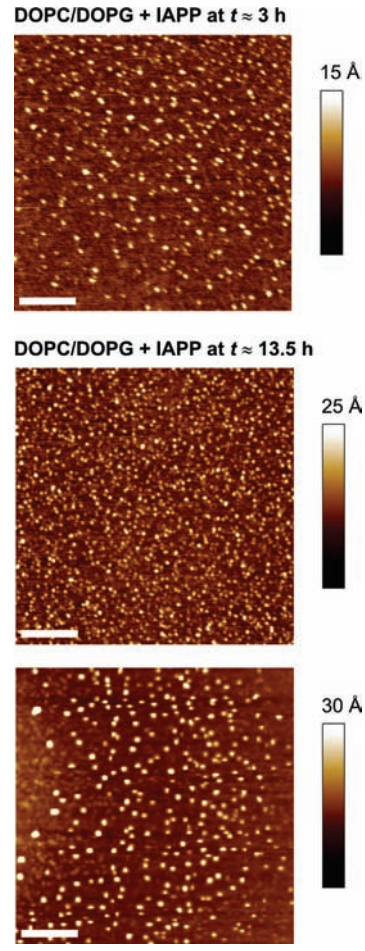

Figure 2. AFM images of isolated IAPP species at $t \approx 3$ h and $t \approx 13.5$ h of the X-ray reflectivity experiments on 1 μM IAPP at the anionic DOPC/DOPG lipid interface. The determined mean height ± standard deviation for the early IAPP oligomers in the lipid monolayer at $t \approx 3$ h is 5.2 ± 3.0 Å. At $t \approx 13.5$ h, larger oligomeric structures can be detected showing a mean height of 7.1 ± 2.6 Å (middle image) and 26.7 ± 10.2 Å (lower image). In the AFM images, the vertical color scale from dark brown to white corresponds to an overall height of 15, 25, and 30 Å for the upper, middle, and lower image, respectively; the scale bar included corresponds to 3000 Å.

AFM measurements were performed on a MultiMode scanning probe microscope with a NanoScope IIIa controller (Digital Instruments, Santa Barbara, CA) and usage of an E-Scanner (scan size 15 μm; Veeco Instruments, Mannheim, Germany).[25] Images were obtained by applying the Tapping Mode in air with silicon SPM sensors from Nanosensors (PPP-NCHR, NanoAndMore, Wetzlar, Germany). Tips with nominal force constants of 42 N·m^{-1} were used at driving frequencies around 290 kHz and drive amplitudes between 35 and 109 mV. Height and amplitude images of sample regions were acquired with resolutions of 512 × 512 pixels and scan frequencies between 0.75 and 1.5 Hz. All measurements were carried out at room temperature. For image analysis and processing, the softwares NanoScope version 5, Gwyddion version 2.10, and Origin were used.

2.5. Attenuated Total Reflection Fourier-Transform Infrared (ATR-FTIR) Spectroscopy. The peptide was dissolved in HFIP to disaggregate the peptide, followed by the removal of

(22) Russell, T. P. *Mater. Sci. Rep.* **1990**, *5*, 171–271.
(23) Tolan, M. *X-Ray Scattering from Soft Matter Thin Films*; Springer: Berlin, 1999.
(24) Seeck, O. H.; Kaendler, I. D.; Tolan, M.; Shin, K.; Rafailovich, M.; Sokolov, J.; Kolb, R. *Appl. Phys. Lett.* **2000**, *76*, 2713–2715.
(25) Jansen, R.; Dzwolak, W.; Winter, R. *Biophys. J.* **2005**, *88*, 1344–1353.

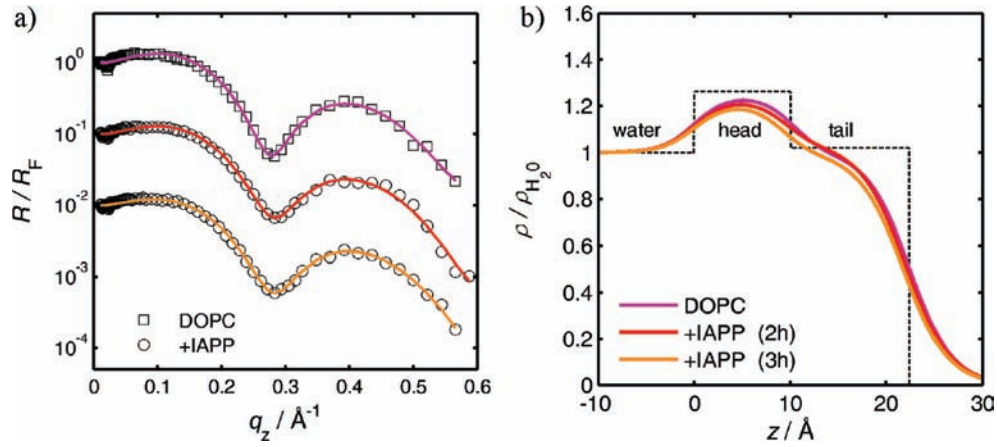

Figure 3. (a) X-ray reflectivity data and (b) normalized electron density profiles for the neutral (zwitterionic) DOPC monolayer and its interaction with IAPP.

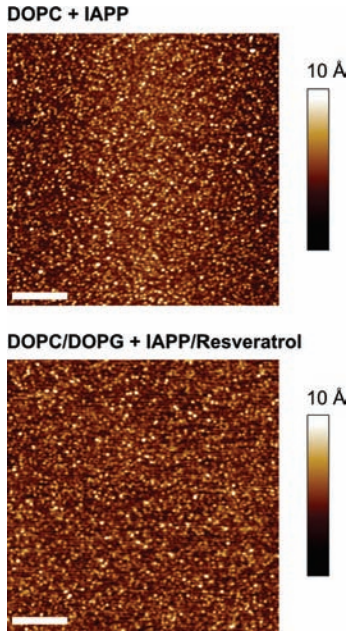

Figure 4. AFM images of isolated IAPP species at particular time points of the X-ray reflectivity experiments. In the presence of a zwitterionic DOPC lipid monolayer, no aggregation of IAPP is observed after 4 h and IAPP monomers can be detected showing a mean height of 3.8 ± 1.8 Å. Similar IAPP species can be detected in the presence of an anionic DOPC/DOPG lipid monolayer when stoichiometric concentrations of resveratrol (1 μM) were added, indicating an inhibitory effect of resveratrol at the early stages of IAPP aggregation. The determined mean height ± standard deviation for the nonreactive IAPP/resveratrol complexes is 3.8 ± 1.2 Å (isolation of the species was carried out after 5 h). In the AFM images, the vertical color scale from dark brown to white corresponds to an overall height of 10 Å; the scale bar corresponds to 3000 Å.

solvent by lyophilization. Reconstitution in buffer (1 mL) and shaking (Vortexer) yielded a 10 μM solution. Stock solutions of the lipids were prepared by dissolving a mixture of DOPC (7 mg) and DOPG (3 mg) in $CHCl_3$ up to a concentration of 10 mg·mL^{-1}. This solution (50 μL), which contained 0.5 mg of lipids, was dried under a stream of N_2. To remove residual solvent, the samples were placed in a Speed-Vac for 3 h. The DOPC/DOPG (7:3; 0.5 mg) mixture was dissolved in buffer (1 mL) and ultrasonicated for 10 min. After five freeze−thaw cycles, a homogeneous solution of multilamellar vesicles (MLV) was obtained. To obtain large, unilamellar vesicles (LUV), the solution was passed through an extruder with a membrane filter made of polycarbonate (11×; pore

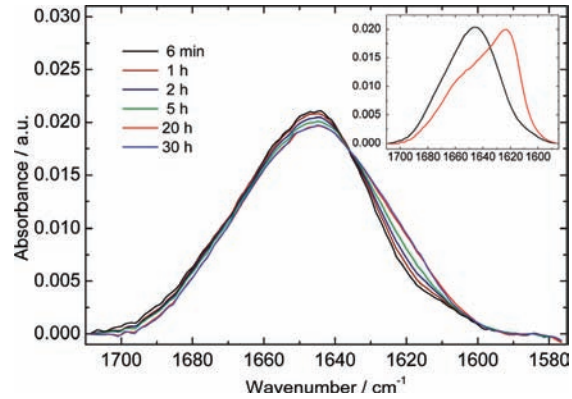

Figure 5. Time course of ATR-FTIR spectra of the amide-I′ band of 10 μM IAPP in the presence of a DOPC supported lipid bilayer. The spectra were normalized to the peak area between 1710 and 1585 cm^{-1}. The inset shows corresponding data for 10 μM IAPP in the presence of the negatively charged DOPC/DOPG (7:3) membrane, which reveals strong IAPP aggregation and fibril formation after 20 h (red curve).

diameter: 0.1 μm). For all FTIR spectroscopic experiments, a phosphate buffer (10 mM, pH 7.4) in D_2O, which contained NaCl (total ionic strength 100 mM), was used.

ATR-FTIR spectra were recorded using a Nicolet 6700 infrared spectrometer at a spectral resolution of 2 cm^{-1}. The ATR out-of-compartment accessory consists of a liquid jacketed Piketech ATR flow-through cell with a trapezoidal Ge-Crystal (Piketech, Madison, WI, 80 × 10 × 4 mm, angle of incidence: 45°). The freshly prepared solution of large unilamellar vesicles was injected into the ATR-flow-cell, which was held at 25 °C; this led to the spontaneous formation of supported lipid bilayers on the surface of the Ge crystal used. Adsorption of the membrane was controlled by following the increase of the CH_2 lipid band intensities over time. After adsorption overnight, the membrane was washed with buffer over 6 h. To ensure integrity of the membrane, the IAPP and IAPP-inhibitor solutions were injected into the ATR cell by means of a peristaltic pump at 1.4 mL·min^{-1}. Spectra were processed using GRAMS software (Thermo Electron). After subtraction of buffer together with the membrane and noise, the spectra were baseline corrected between 1710 and 1585 cm^{-1} and normalized to the amide-I′ band area (also between 1710 and 1585 cm^{-1}).

3. Results and Discussion

The X-ray reflectivity data of the DOPC/DOPG lipid film in the presence of IAPP (Figure 1a) reveal marked IAPP-induced

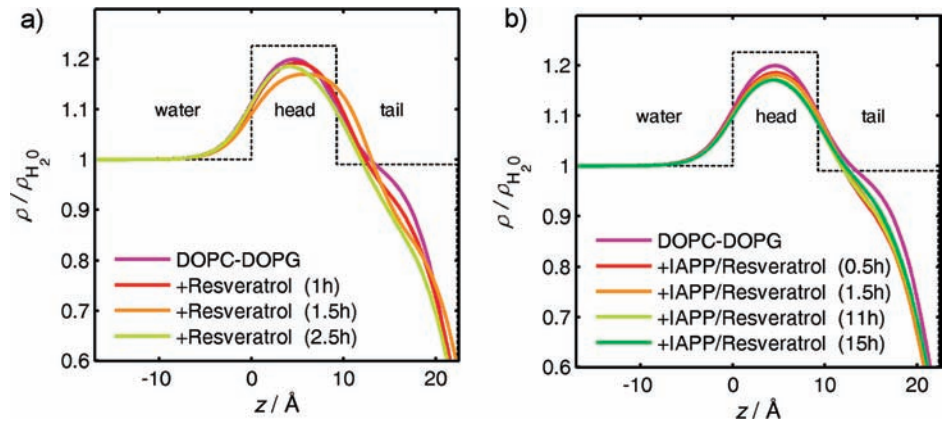

Figure 6. (a) Normalized electron density profiles of the negatively charged DOPC/DOPG membrane in the presence of resveratrol at different times (time evolution: resveratrol dissolved in the bulk solvent, adsorption to the lipid headgroup area, partial penetration into the upper chain region). (b) Time evolution of the electron density profile of the lipid film in the presence of 1.5 μM resveratrol and 1 μM IAPP. The primary XRR data are shown in the Supporting Information.

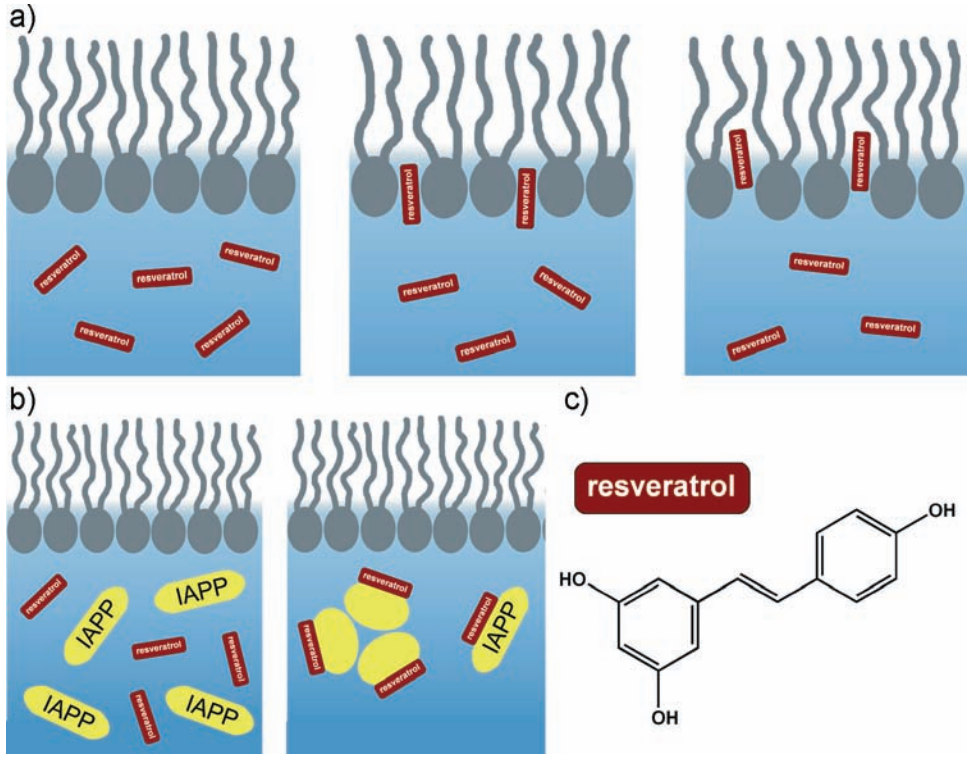

Figure 7. Schematic illustration of (a) how resveratrol perturbs the lipid monolayer structure and (b) the inhibitory effect of resveratrol on IAPP fibrillation as revealed from the combined XRR, ATR-FTIR spectroscopic and AFM data. (c) Chemical structure of resveratrol.

changes for the intermediate time range. Inspection of the time-evolution of the electron density profiles (Figure 1b) shows that right after preparation of the 1 μM IAPP solution, a film thickness of 22 Å is observed, which is consistent with the thickness of the pure lipid film. Thereafter, $\rho(z)$ of the headgroup and lipid chain region changes, indicating insertion of IAPP into the lipid's upper chain region, where the aggregation process via oligomerization is initiated, which is followed by an increase of $\rho(z)$ in the tail region. Integration of the electron density for -10 Å $< z <$ 30 Å indicates that the size of the IAPP oligomers is restricted to ~20 Å. After 3 h, the maximal thickness of the IAPP layer observed by XRR is roughly 13 Å. The time-dependent oligomerization of IAPP in the presence of the aggregation-fostering, anionic DOPC/DOPG lipid monolayer has also been observed by AFM (Figure 2). To reveal morphological details of IAPP in the DOPC/DOPG monolayer after 3 h, the lipid film was carefully removed from the aqueous subphase in the Langmuir trough and the existing IAPP species were isolated. The determined mean height ± standard deviation for the early IAPP oligomers in the lipid monolayer is 5.2 ± 3.0 Å. Finally, after several hours, when the IAPP aggregates have grown bigger, the electron density profile of the pure lipid film is restored, indicating that the larger IAPP aggregates do not perturb the lipid film anymore, but rather detach from the lipid phase and enter the bulk solution (Figure 1c). An investigation of the bulk solution by AFM revealed that after 13.5 h the existing IAPP oligomers had mean heights from 7.1 ± 2.6 Å (Figure 2, middle image) to 26.7 ± 10.2 Å (Figure 2, lower image). If

the IAPP concentration is high enough (>5 μM), also fibrils are formed (Figure 1C, Supporting Information).[11,15,16,26]

For comparison, we also studied the interaction of IAPP with a neutral, zwitterionic DOPC lipid monolayer. The reflectivity data (Figure 3) reveal that the structure of the DOPC lipid layer is not significantly affected in the presence of IAPP. This can be attributed to the absence of an electrostatically driven interaction between the positively charged IAPP and the anionic lipid interface, in agreement with recent IRRAS spectroscopic studies.[11] This clearly shows that the initial association of IAPP with lipid membranes is mainly driven by electrostatic interactions.[10,11] The small changes in the electron density profile (Figure 3b) with time are probably due to minor reorganization processes in the region of the lipid chains. In bulk solution, a large amount of very small peptide particles could be found by AFM in the presence of the zwitterionic DOPC lipid monolayer only (Figure 4). The average particle height was 3.8 $\pm$ 1.8 Å, indicating the prevailing presence of IAPP monomers. The largest particles observed had heights of $\sim$10 Å.

The scenario observed for IAPP in the presence of the zwitterionic DOPC membrane was further confirmed by ATR-FTIR spectroscopic measurements. Figure 5 displays the time evolution of ATR-FTIR spectra of the amide-I′ band region after a solution of 10 μM IAPP was injected into the ATR-FTIR cell, which already contained a supported bilayer film of DOPC. The peak maximum of the amide-I′ band appears at $\sim$1645 cm^{-1}, which can be attributed to unordered secondary structures. Within the time course of 20 h, a small shoulder around $\sim$1620 cm^{-1} is formed, indicating minor changes of the secondary structure of adsorbed IAPP. In the next 10 h, the structure does not evolve any further, leading to the conclusion that IAPP in the presence of the zwitterionic DOPC membranes partially adsorbs but remains mainly unordered. For comparison, the amide-I′ band of IAPP in the presence of the anionic DOPC/DOPG bilayers undergoes a strong shift of the peak maximum from $\sim$1646 cm^{-1} toward 1623 cm^{-1} (Figure 5, inset). In this case, the peptide is fully aggregating, displaying an amide-I′ band which is typical for intermolecular β-sheet formation.

Finally, the interaction of resveratrol with the lipid membrane has been examined in the absence and presence of IAPP. The corresponding electron density profiles $\rho(z)$ are displayed in Figure 6a,b. For the lipid/resveratrol system, we initially observe an intact lipid film which is not perturbed by the small molecule. Subsequently, changes of $\rho(z)$ in the lipid headgroup and chain region are detected, indicating a decrease of lipid chain packing by migration of resveratrol in the upper chain region passing the lipid headgroup area (Figure 7a). Figures 6b and 7b reveal the corresponding effect upon addition of IAPP. Different from the pure IAPP/lipid system (Figure 1b), no aggregation of IAPP is observed at the lipid interface and no marked adsorption of resveratrol at the lipid interface is detected anymore. Hence, we may conclude that resveratrol and IAPP interact essentially in the bulk solution, so that the N-terminus of IAPP is masked in such a way that interaction with the aggregation-fostering membrane and, consequently, amyloid formation do not occur. In fact, essentially very small IAPP particles, probably consisting of nonreactive resveratrol/IAPP complexes, are found in the bulk phase using atomic force microscopy, only (Figure 4). The average particle height of these species is 3.8 $\pm$ 1.2 Å with largest particle heights of $\sim$10 Å. Hence, the IAPP particles detected in the presence of the fibrillation inhibitor resveratrol are probably largely identical with IAPP monomers, indicating that resveratrol inhibits the aggregation of IAPP effectively and already at the very initial stage of the aggregation/fibrillation process. In the presence of IAPP, no effect of resveratrol on the structural properties of the lipid layer can be observed anymore. This reveals that the interaction with IAPP is much stronger and preferred over the interaction with the lipid membrane, indicating a marked interaction of the largely hydrophobic resveratrol with the peptide which seems to be more favorable than the interaction with the hydrophilic (charged) lipid headgroup region of the lipid layer, which has to be penetrated to access the preferred hydrophobic chain region of the membrane.

4. Conclusions

To conclude, first XRR studies on IAPP at lipid interfaces have been carried out, providing a molecular picture of the time-dependent scenario occurring upon aggregation of IAPP at anionic lipid interfaces. The lipid interface essentially serves as nucleation center for IAPP aggregation only. After growth of larger structures, the peptide aggregates are released to the bulk, where, at IAPP concentrations higher than $\sim$5 μM, growth of large fibrils takes place. Moreover, we show that the polyphenolic red wine compound resveratrol is able to inhibit IAPP aggregation also in the presence of aggregation-fostering negatively charged lipid interfaces. Inhibition takes place during the very early stages of the fibrillogenesis and is efficient already at stoichiometric concentrations of resveratrol and IAPP.

Acknowledgment. Financial support from the DFG and the BMBF is gratefully acknowledged. We thank HASYLAB for providing synchrotron radiation.

Supporting Information Available: Additional data: experimental setup; X-ray reflectivity data of the negatively charged DOPC/DOPG monolayer and its interaction with IAPP and resveratrol; X-ray reflectivity data on the interaction of resveratrol with this lipid system; inhibitory effect of resveratrol on IAPP aggregation; tables of parameters retrieved from fitting the reflectivity data of the DOPC/DOPG membrane system in the presence of IAPP, resveratrol, and both IAPP and resveratrol. This material is available free of charge via the Internet at http://pubs.acs.org.

JA8097417

(26) Padrick, S. B.; Miranker, A. D. *Biochemistry* **2002**, *41*, 4694–4703.